In vivo bioluminescence imaging reveals copper deficiency in a murine model of nonalcoholic fatty liver disease

Marie C. Heffern[a,1], Hyo Min Park[b,1], Ho Yu Au-Yeung[a,1,2], Genevieve C. Van de Bittner[a,3], Cheri M. Ackerman[a], Andreas Stahl[b,4], and Christopher J. Chang[a,c,d,e,4]

[a]Department of Chemistry, University of California, Berkeley, CA 94720; [b]Department of Nutritional Sciences and Toxicology, University of California, Berkeley, CA 94720; [c]Department of Molecular and Cell Biology, University of California, Berkeley, CA 94720; [d]Helen Wills Neuroscience Institute, University of California, Berkeley, CA 94720; and [e]Howard Hughes Medical Institute, University of California, Berkeley, CA 94720

Edited by Harry B. Gray, California Institute of Technology, Pasadena, CA, and approved November 9, 2016 (received for review August 16, 2016)

Copper is a required metal nutrient for life, but global or local alterations in its homeostasis are linked to diseases spanning genetic and metabolic disorders to cancer and neurodegeneration. Technologies that enable longitudinal in vivo monitoring of dynamic copper pools can help meet the need to study the complex interplay between copper status, health, and disease in the same living organism over time. Here, we present the synthesis, characterization, and in vivo imaging applications of Copper-Caged Luciferin-1 (CCL-1), a bioluminescent reporter for tissue-specific copper visualization in living animals. CCL-1 uses a selective copper(I)-dependent oxidative cleavage reaction to release D-luciferin for subsequent bioluminescent reaction with firefly luciferase. The probe can detect physiological changes in labile Cu^{+} levels in live cells and mice under situations of copper deficiency or overload. Application of CCL-1 to mice with liver-specific luciferase expression in a diet-induced model of nonalcoholic fatty liver disease reveals onset of hepatic copper deficiency and altered expression levels of central copper trafficking proteins that accompany symptoms of glucose intolerance and weight gain. The data connect copper dysregulation to metabolic liver disease and provide a starting point for expanding the toolbox of reactivity-based chemical reporters for cell- and tissue-specific in vivo imaging.

metal homeostasis | molecular imaging | luciferin | metabolic liver disease | copper

Copper is an essential mineral for all higher organisms, serving as a redox-active cofactor for physiological processes, including respiration (1, 2), antioxidant defense (3, 4), neurotransmitter synthesis and metabolism (5), epigenetic modifications (6), and emerging roles in dynamic signaling networks (7–11). This same redox activity also poses a potential danger, requiring highly orchestrated regulation of copper pools to prevent oxidative stress and free radical damage events that are detrimental to health (12–18). Indeed, genetic disorders that disrupt copper homeostasis lead to severe and lethal conditions such as Menkes and Wilson's diseases (13, 19, 20), and imbalances in physiological copper levels and tissue miscompartmentalization arising from genetic and/or dietary factors are correlated with cancer, neurodegenerative diseases, and metabolic disorders such as obesity, diabetes, and nonalcoholic fatty liver disease (NAFLD) (21–32).

This central importance of copper in biology motivates the development of technologies to enable monitoring of labile, loosely bound copper pools in living systems to disentangle contributions of global (whole animal) and/or local (tissue specific) copper dynamics in healthy and disease states (9, 16, 33). However, the vast majority of these tools have been limited to dissociated cell culture and related thin specimens (e.g., zebrafish), and current examples of in vivo copper imaging in mammalian models remain rare owing to the challenges of coupling a selective and sensitive response to copper with modalities that offer tissue penetration at appropriate depths (16, 34–39). Moreover, none of these technologies allow for in vivo copper imaging in a targeted cell- or tissue-specific manner.

Here we present a bioluminescent reporter system for imaging copper in a living animal model system that couples the high selectivity, sensitivity, and chemical tunability of a small-molecule chemical probe with the tissue specificity afforded by a genetically engineered mouse model. Copper-Caged Luciferin-1 (CCL-1) is a tris[(2-pyridyl)-methyl]amine (TPA) ligand caged probe that generates D-luciferin upon oxidative cleavage with Cu^{+} for subsequent reaction with firefly luciferase to produce a bioluminescent response. Because the luciferase enzyme required for bioluminescent signal generation is genetically encodable, this reporter system can enable copper imaging in specific cell and tissue populations in the same animal over time. As such, CCL-1 represents a first-generation probe for reactivity-based copper imaging in vivo, and, to the best of our knowledge, for any endogenous biological metal. We establish the ability of CCL-1 to detect changes in the physiological range of labile copper pools in living cells and mice under basal, copper-overload, and copper-deficient conditions with

Significance

Like all essential metals in mammals, deficiency or excess of copper can be detrimental to health. We present a bioluminescent reporter based on copper-dependent uncaging of a D-luciferin substrate for selective, sensitive, and tissue-specific longitudinal imaging of labile copper pools in animal model systems. Application of this technology to monitor a diet-induced mouse model of nonalcoholic fatty liver disease, a disorder affecting *ca.* 100 million Americans, reveals hepatic copper deficiency and altered expression levels of copper homeostatic proteins that accompany glucose intolerance and weight gain. The results demonstrate the viability of this molecular imaging approach and connect copper dysregulation to metabolic liver disease, providing a platform for designing reactivity-based reporters for cell- and tissue-specific in vivo metal imaging.

Author contributions: M.C.H., H.M.P., H.Y.A.-Y., G.C.V.d.B., A.S., and C.J.C. designed research; M.C.H., H.M.P., H.Y.A.-Y., G.C.V.d.B., and C.M.A. performed research; H.Y.A.-Y. and C.M.A. contributed new reagents/analytic tools; M.C.H., H.M.P., H.Y.A.-Y., and G.C.V.d.B. analyzed data; and M.C.H., H.M.P., H.Y.A.-Y., G.C.V.d.B., C.M.A., A.S., and C.J.C. wrote the paper.

The authors declare no conflict of interest.

This article is a PNAS Direct Submission.

[1]M.C.H., H.M.P., and H.Y.A.-Y. contributed equally to this work.

[2]Present address: Department of Chemistry, The University of Hong Kong, Hong Kong, People's Republic of China.

[3]Present address: Agilent Research Laboratories, Agilent Technologies, Santa Clara, CA 95051.

[4]To whom correspondence may be addressed. Email: chrischang@berkeley.edu or astahl@berkeley.edu.

This article contains supporting information online at www.pnas.org/lookup/suppl/doi:10.1073/pnas.1613628113/-/DCSupplemental.

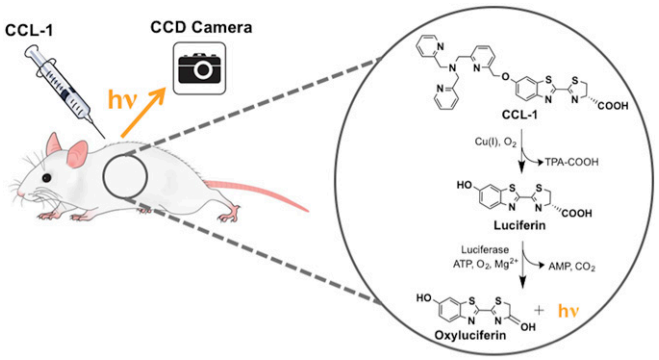

Fig. 1. Design of CCL-1 through selective Cu^+-mediated oxidative release of the D-luciferin substrate.

high selectivity and sensitivity, including targeted visualization of hepatic copper stores using a liver-specific luciferase-expressing mouse. We apply this unique technology to monitor copper status during progression of a diet-induced murine model of NAFLD, revealing onset of hepatic copper deficiency and alterations in central copper homeostasis proteins that accompany symptoms of glucose intolerance and weight gain. Taken together, this work provides an example of monitoring copper dynamics in a longitudinal manner over the course of NAFLD disease acquisition, connecting copper dysregulation to metabolic liver disease. The data demonstrate the feasibility of combining chemical design with bioengineering for tissue-specific imaging of essential metals in living animals, affording a starting point for interrogating the bioinorganic chemistry in disease pathology with molecular bioluminescence imaging.

Results and Discussion

Design and Synthesis of CCL-1. Luciferin-based bioluminescence imaging is an attractive modality for in vivo use owing to its low background signal, efficient photon production, and good tissue penetration of its red-shifted emission (40–42). Moreover, impressive advances in luciferase engineering and ease of targeting by genetic encoding permit the broad use of such reporters for in vivo imaging with cell and tissue specificity (41, 43, 44). We and others have developed caged luciferins, which are enzyme-inert luciferin derivatives that are chemically unmasked to the luciferin substrate in the presence of an analyte or biochemical event of interest for subsequent enzymatic generation of light (45–50); in particular, our laboratory has used this approach to develop bioluminescent H_2O_2 reporters (45, 47). To create a Cu^+-responsive luciferin probe, we exploited a Cu^+-dependent oxidative cleavage reaction mediated by the tetradentate ligand TPA (Fig. 1), inspired by the use of this pendant to develop a Cu^+-selective fluorescent probe (51) as well as work from our laboratory on related metal-dependent oxidations for fluorescence detection of Co^{2+} and Fe^{2+} in living cells (52, 53). The synthesis of CCL-1 based on this design strategy is depicted in Scheme 1 and offers a general and versatile platform for appending other potential ligands to tune metal specificity and reactivity.

Reactivity and Selectivity of CCL-1 to Copper. Cu^+-mediated luminescence production from CCL-1 was initially evaluated in aqueous buffer (50 mM Tris at pH 7.4, 5 mM glutathione). First, a 5-μM solution of CCL-1 was incubated with various concentrations of Cu^+ (0.5 μM to 50 μM) to mimic the physiological range of copper for 1 h, followed by addition of recombinant firefly luciferase. Luminescent signal production was monitored with a plate reader and compared with control samples without added Cu^+. As shown in Fig. 2*A*, a good correlation between Cu^+ concentration and total bioluminescent signal was observed up to 5 μM of Cu^+ (1 eq) with signal saturation at higher Cu^+ concentrations, indicating that CCL-1 can reliably detect changes in levels of Cu^+ in a dose-dependent manner. Notably, a *ca.* 80-fold bioluminescence increase was observed upon addition of 1 eq of Cu^+, demonstrating the high signal-to-noise response of the probe. Time-dependent studies establish the ability of probe to detect dynamic changes in Cu^+ fluxes (*SI Appendix*, Fig. S1), showing a >10-fold increase in bioluminescence intensity within 5 min of adding 1 eq of Cu^+. Reaction of CCL-1 with a higher concentration of Cu^+ (20 eq) resulted in a much faster response, with a >80-fold signal increase observed after a 20-min incubation time. The resulting bioluminescent product was stable in serum-containing media over a 24-h period (*SI Appendix*, Fig. S2). Moreover, CCL-1 is selective for Cu^+ compared with a panel of biologically relevant metal ions, including Mg^{2+}, Ca^{2+}, and Zn^{2+}, as well as other common first-row transition metal ions (Fig. 2*B*). The copper-selective response is not observed in control experiments with D-luciferin, indicating that the observed reactivity of CCL-1 is not a result of altered luciferase activity (*SI Appendix*, Fig. S3). Only free Co^{2+} gives a modest response to CCL-1; however, although biological concentrations of loosely bound ionic Co^{2+} are not well studied, the concentration tested here is not considered physiologically relevant, as most Co^{2+} are found tightly bound to proteins. As an additional experiment, we tested the response of CCL-1 with cobalamin (vitamin B_{12}), the tightly bound form in which Co^{2+} is primarily found in mammalian systems under physiological conditions. As expected, CCL-1 exhibited no detectable response to vitamin B_{12}. Finally, to simulate the reducing intracellular environment, 5 mM GSH was used in the buffer media. Under such conditions, Cu^{2+} was readily reduced to Cu^+, and thus the addition of this metal salt in the presence of the glutathione (GSH) reductant leads to a comparable bioluminescent enhancement (*ca.* 70-fold) to that observed when adding Cu^+ alone.

CCL-1 Detects Changes in Labile Copper Levels in Living Cells. After establishing that CCL-1 can reliably monitor a range of different Cu^+ levels in aqueous buffer, the utility of the probe for detection of labile Cu^+ in live cells was tested. Two luciferase-expressing cell lines, PC3M-luc and LNCaP-luc, were used in these experiments. The cells were supplemented with different concentrations of $CuCl_2$ for 24 h to raise intracellular levels of labile copper, washed with fresh buffer containing no added copper, and then treated with CCL-1. The data in Fig. 2 *C* and *D* and *SI Appendix*, Fig. S4*B* reveal increases in bioluminescence intensity from CCL-1 that correlate with increasing concentrations of added $CuCl_2$ in a dose-dependent manner, which is not observed when cells are imaged with D-luciferin alone (*SI Appendix*, Fig. S5). In the presence and absence of copper treatment, signal was immediately generated, and peaked at ∼15 min, then decayed down to negligible signal from 15 min to 55 min (*SI Appendix*, Fig. S4*A*). Similar flash-type light emission kinetics are observed with D-luciferin, where the decay results from enzyme inhibition by luciferin/luciferase reaction byproducts (41, 42, 44). The similarity in light emission kinetics in the presence and absence of copper

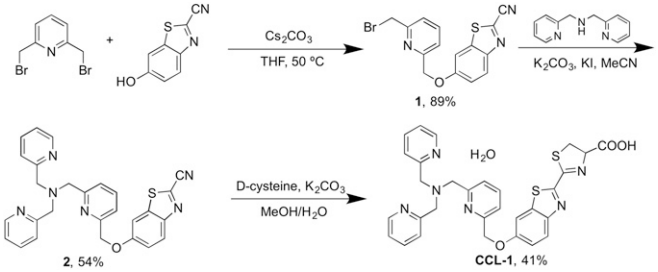

Scheme 1. Synthesis of CCL-1.

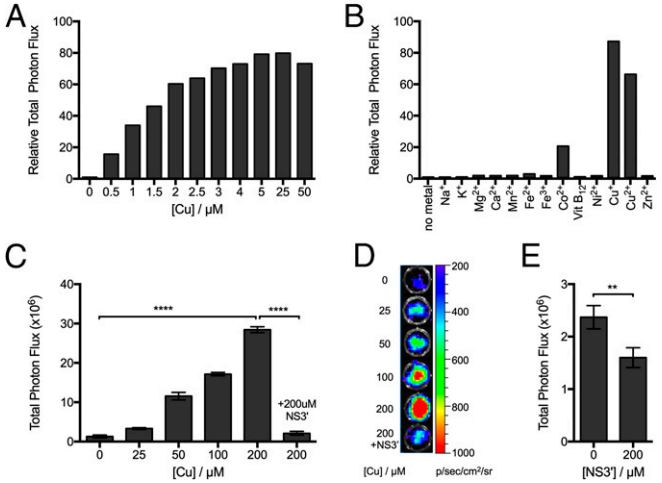

Fig. 2. CCL-1 selectively responds to Cu^+ and can measure dynamic changes in Cu^+ levels in living cells. Relative bioluminescence response of CCL-1 (5 μM, in 50 mM Tris, pH 7.4, 5 mM GSH) after 1 h incubation with (*A*) varying concentrations of Cu^+ and (*B*) various biologically relevant s-block (1 mM) and d-block (100 μM) metal ions and cobalamin (vitamin B_{12}). Signals are integrated over 1 h and expressed as relative photon fluxes normalized to CCL-1 bioluminescence with no metal ion treatment. (*C*) Bioluminescent signals from PC3M-luc cells probed with CCL-1. Cells were supplemented with $CuCl_2$ for 24 h, followed by addition of CCL-1 (25 μM) ± the membrane-permeable copper chelator NS3′ (200 μM). Total photon flux was integrated over 2 h. Statistical analyses were performed with a two-tailed Student's *t* test. $^{****}P \leq 0.0001$, and error bars are ±SD ($n = 3$). (*D*) Representative images of PC3M-luc cells treated with $CuCl_2$ and imaged with CCL-1. (*E*) Bioluminescent signals from PC3M-luc cells ± NS3′ (200 μM) and imaged with CCL-1 (50 μM). Total photon flux was integrated over 2 h. Statistical analyses were performed with a two-tailed Student's *t* test. $^{**}P \leq 0.01$, and error bars are ±SD ($n = 3$).

treatment suggests that bioluminescence results from luciferase reaction with the same substrate, namely D-luciferin.

The bioluminescent signal was reversibly attenuated to basal levels when cells were treated with the intracellular Cu^+ chelator, tris[2-(ethylthio)ethyl]amine (NS3′) before addition of CCL-1, further verifying that the observed increases in bioluminescence are copper-dependent. Finally, PC3-luc cells were treated with NS3′ alone to reduce the endogenous level of labile intracellular copper. These cells exhibited a significant decrease in bioluminescence compared with control cells, indicating that CCL-1 is sensitive enough to detect basal, endogenous pools of labile copper (Fig. 2*E*). In contrast, imaging PC3-luc cells with D-luciferin under the same conditions does not result in any noticeable change in bioluminescence signal (*SI Appendix*, Fig. S6). Taken together, the results establish that CCL-1 can report on dynamic changes in labile Cu^+ levels in living cells in situations of copper excess or deficiency, including alterations in copper pools at physiological levels.

CCL-1 Visualizes Changes in Exchangeable Copper Pools in Living Mice. We next turned our attention to monitoring changes in labile copper pools in living animals. Initial studies used firefly luciferase-expressing FVB-luc$^+$ mice, where luciferase expression is driven by the actin promoter and is thus present in the majority of the organs within these animals. At basal levels of copper (no treatment), mice were injected with CCL-1, and light production was monitored for 1 h to determine the total photon flux for each animal. Injection of mice with different doses of CCL-1 resulted in differences in bioluminescent signal intensities that were dependent on the dose of the probe at the range tested (25 nmol to 0.4 μmol, *SI Appendix*, Fig. S7*A*), indicating that this range is below the saturation limit. We further determined that at 0.2 μmol of CCL-1, CCL-1 is metabolically cleared with similar kinetics to the parent D-luciferin (*SI Appendix*, Fig. S8).

To determine the response of CCL-1 to in vivo alterations in copper levels, mice were treated with vehicle or a sublethal dose of $CuCl_2$ (i.p., 3 mg/kg) for 2 h before injection of 0.2 μmol of CCL-1 (Fig. 3). Animals pretreated with this dose of copper showed a robust, ninefold increase in bioluminescence intensity from CCL-1 compared with controls. The copper-dependent increase in bioluminescent signal intensity was similarly observed in mice imaged at low doses (25 nmol) and high doses (0.4 μmol) of CCL-1 (*SI Appendix*, Fig. S7*C*), suggesting that increases in copper levels can be detected across a wide range of probe concentrations. Additionally, pretreatment of mice with different amounts of $CuCl_2$ and imaged with 0.2 μmol of CCL-1 showed a dose-dependent increase in signal as a function of copper concentration (*SI Appendix*, Fig. S7*B*).

To verify whether this change in bioluminescent signal was indeed copper-dependent, animals exposed to $CuCl_2$ or vehicle were additionally treated with the copper chelator ATN-224 (5 mg/kg) before injection of CCL-1 (Fig. 3 and *SI Appendix*, Fig. S7*A*). The intensities of bioluminescent signals observed from animals treated with both $CuCl_2$ and chelator were comparable to those of the control group, and those treated with chelator alone showed decreases in signal from basal levels. The alterations in bioluminescence response in mice treated with copper or copper chelators indicate that CCL-1 can monitor fluctuations in copper levels in vivo. No significant differences in bioluminescence were observed between mice similarly injected with vehicle, $CuCl_2$, and $CuCl_2$/ATN-224 and imaged with D-luciferin, attributing the copper-dependent response of CCL-1 to the presence of the TPA ligand cage (*SI Appendix*, Fig. S9).

As the liver is a central organ for copper storage and homeostatic regulation, we next sought to image hepatic copper with CCL-1 in mice expressing luciferase under the control of the albumin promoter for liver-specific luciferase expression, termed L-Luc mice. The mice were generated by crossing mice bearing the *Gt(ROSA)26Sor*$^{tm1(Luc)Kael}$ allele and Tg(Alb-cre)21Mgn mice (54). In a similar protocol as was used for the FVB-luc$^+$ mice, the L-Luc mice were first treated with vehicle (Dulbecco's phosphate-buffered saline), $CuCl_2$ (3 mg/kg), or both ATN-224 (5 mg/kg) and $CuCl_2$ (Fig. 4). Injection of L-Luc mice with CCL-1 showed bioluminescent signals specifically in the liver (*SI Appendix*, Fig. S10). Copper treatment of L-Luc mice resulted in a sevenfold increase in bioluminescent signal from CCL-1, and this increase was attenuated by treatment with ATN-224, demonstrating the ability of the reporter to detect rises in hepatic copper levels in situations of copper excess. As a number of metabolic disorders have been reported to result in copper

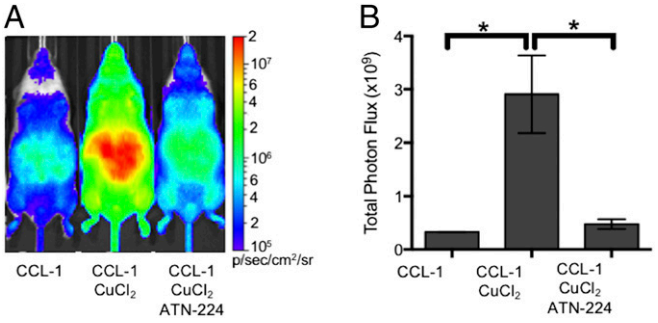

Fig. 3. CCL-1 monitors labile copper dynamics in luciferin-expressing mice. FVB-luc$^+$ mice were injected (i.p.) with CCL-1 (0.2 μmol) after i.p. injection of vehicle, $CuCl_2$ (3 mg/kg), or both $CuCl_2$ (3 mg/kg) and ATN-224 (5 mg/kg). Injections of $CuCl_2$ and ATN-224 were performed 2 h and 10 min, respectively, before injection CCL-1. (*A*) Representative images of FVB-luc$^+$ mice injected with CCL-1. (*B*) Total photon flux, 0–60 min postinjection. Statistical analyses were performed with a two-tailed Student's *t* test. $^*P < 0.05$ ($n = 3$–5), and error bars are ±SEM.

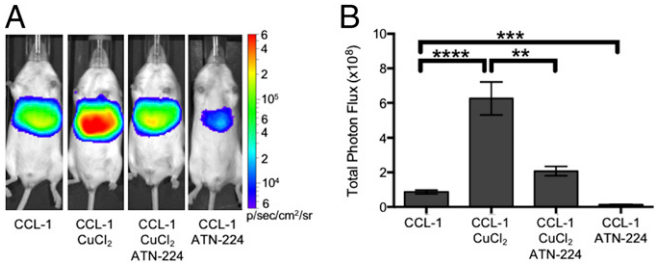

Fig. 4. CCL-1 monitors Cu^{+} dynamics and can detect endogenous, basal labile Cu^{+} levels in L-Luc mice. L-Luc mice were injected (i.p.) with CCL-1 (0.1 μmol) after i.p. injection of vehicle, $CuCl_2$ (3 mg/kg) alone, both $CuCl_2$ (3 mg/kg) and ATN-224 (5 mg/kg), or ATN-224 (30 mg/kg) alone. Injections of $CuCl_2$ or ATN-224 alone were performed 2 h before injection of CCL-1. Mice injected with both $CuCl_2$ and ATN-224 were injected 2 h and 10 min, respectively, before injection of CCL-1. (*A*) Representative images of L-Luc mice injected with CCL-1 under various conditions. (*B*) Total photon flux, 0–60 min postinjection. Statistical analyses were performed with a two-tailed Student's *t* test. $^{**}P \leq 0.01$, $^{***}P \leq 0.001$, $^{****}P \leq 0.0001$ ($n = 3$–7), and error bars are ±SEM.

deficiency, we treated another group of mice with ATN-224 alone (30 mg/kg) to reduce copper levels before imaging (Fig. 4). As expected, chelator-treated mice show a *ca.* 6.5-fold decrease in bioluminescent signal intensity compared with the basal vehicle controls, establishing that CCL-1 is capable of detecting both depletion and overload of labile copper pools specifically in hepatic tissue in living animals. In agreement with experiments performed in FVB-luc^{+} mice, no copper-dependent response was observed in L-luc mice imaged with D-luciferin alone (*SI Appendix*, Fig. S11), ruling out potential differences in transport, uptake, or activity of the uncaged luciferin substrate into the liver from peripheral sources under varying copper levels.

CCL-1 Reveals Copper Deficiency with Alterations in Copper Transport Proteins in a Diet-Induced Murine Model of NAFLD. After establishing that CCL-1 can monitor fluctuations in hepatic copper pools in vivo in healthy basal states versus situations of copper deficiency or overload, we sought to apply this indicator to explore potential connections between hepatic copper status and disease. We chose to pursue a diet-induced murine model of NAFLD, owing to its importance as the most common liver disease in developed countries (55–57) and its association with the growing epidemic of obesity and diabetes. Indeed, over 100 million people in the United States alone are afflicted with some form of NAFLD, and ∼20 to 30% of NAFLD cases progress to pathological liver inflammation and cirrhosis, which can lead to liver failure or cancer (58, 59). The exact disease pathology of NAFLD is insufficiently understood, but clinical evidence has linked inadequate copper supply to the disease extent of NAFLD (23–26, 60). Specifically, endpoint assays of total hepatic copper appear to correlate with increased grades of steatosis and circulating free fatty acids in NAFLD patients relative to control subjects (25).

To this end, 6- to 8-wk-old L-Luc mice were either fed a high-fat diet (HFD) to induce NAFLD or maintained on a normal chow (diet on which they were weaned) for 8 wk with weekly monitoring of food intake and weight gain. The particular HFD we selected has been well established to induce hepatic steatosis in a number of mouse strains (61, 62). As expected, at the end of the 8-wk feeding period, the HFD mice showed significant increases in body weight (*ca.* 45%) compared with control mice fed normal chow (*SI Appendix*, Fig. S12). Mice were imaged weekly with D-luciferin to monitor luciferase activity and liver size (*SI Appendix*, Fig. S13), followed by CCL-1 2 d later to measure hepatic copper levels. A group of mice was euthanized 4 wk into the feeding to measure liver size (*SI Appendix*, Fig. S13). Interestingly, a statistically significant decrease in CCL-1 signal normalized to D-luciferin signal was observed in the L-luc mice fed the HFD throughout the 8-wk time period, indicating that the mice develop a hepatic copper deficiency in response to this diet. In contrast, no such decrease was observed in the mice fed normal diets (Fig. 5 *A* and *B*). Notably, a plateau in the decrease of the copper-dependent bioluminescent signal was observed at 4 wk, which represents an intriguing time point, as previous reports

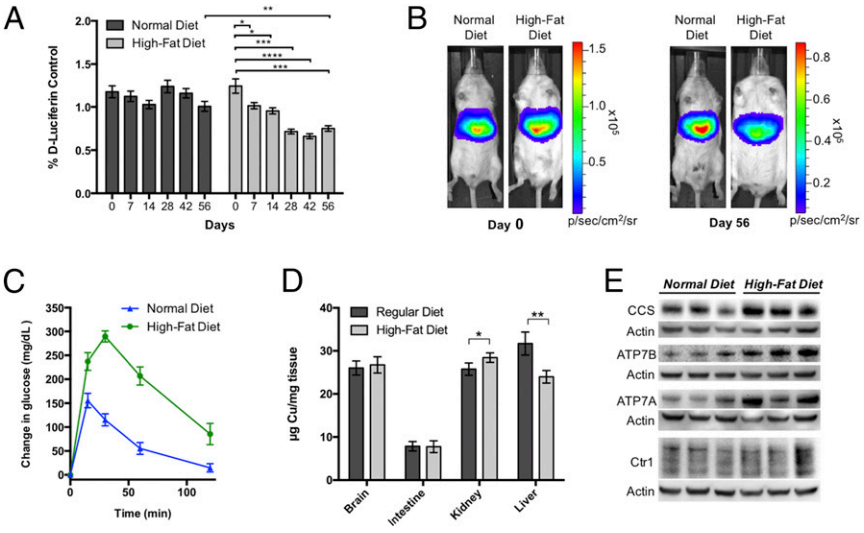

Fig. 5. CCL-1 imaging reveals hepatic copper deficiency in a diet-induced murine model of NAFLD. (*A*) Bioluminescent signal from CCL-1 (normalized to D-luciferin) of L-Luc mice placed on HFD or normal feeding conditions. Mice were imaged biweekly after i.p. injection of D-luciferin followed by CCL-1 2 d later. Error bars are ±SEM ($n \geq 9$), and statistical analyses were performed with a two-tailed Student's *t* test where $^{*}P \leq 0.05$, $^{**}P \leq 0.01$, $^{***}P \leq 0.001$, and $^{****}P \leq 0.0001$. (*B*) Representative images of mice from HFD and normal diet groups before the study (day 0) and at the end of the 8-wk feeding period (day 56). (*C*) Glucose clearance test to monitor glucose intolerance of the two groups of mice following i.p. injection of 200 mg/dL of glucose. Glucose was injected after blood glucose levels were measured at time = 0 min. Data are expressed as changes in glucose levels from basal levels (levels measured at time = 0 min, before glucose injection). Error bars are ±SEM ($n = 6$). (*D*) ICP-MS analysis of total copper in brain, intestine, kidney, and liver tissues from HFD and normal diet groups. Error bars are ±SEM ($n = 6$ or 7), and statistical analyses were performed with a two-tailed Student's *t* test where $^{*}P \leq 0.05$ and $^{**}P \leq 0.01$. (*E*) SDS/PAGE analysis of liver extracts of three mice fed normal diets and three HFD mice. Tissues were probed for CCS, ATP7B, ATP7A, and Ctr1. For Ctr1, the region comprising the unglycosylated (25 kDa) and glycosylated monomer (33–37 kDa) are shown (full blot shown in *SI Appendix*, Fig. S15).

document significant glucose intolerance and metabolic changes in similar diet-dependent mouse models at this time point (61, 62). As an additional control, because of differences in copper in normal diet and HFD, parallel experiments were performed in L-Luc mice fed low-fat diets (LFDs) with equivalent copper levels to the HFD. For these experiments, mice of the same litter and weaned on the normal diet were divided into two groups and fed either the LFD or HFD for 8 wk. Both groups of mice consumed similar amounts of food, but LFD mice did not show significant weight gain compared with mice maintained on normal diets (*SI Appendix*, Fig. S14 *A* and *B*). Furthermore, the bioluminescence signal in the liver from CCL-1 normalized to D-luciferin signal in LFD-fed mice did not exhibit the same decrease observed with the HFD-fed mice (*SI Appendix*, Fig. S14*C*). These data further support that weight gain and reduction in CCL-1 hepatic signal is connected to increased fat consumption in the HFD, suggesting that copper dysregulation may occur before, or perhaps even promote, the onset of symptoms arising from this metabolic disorder.

To provide an independent measure of copper status to correlate with the in vivo copper imaging results, ex vivo tissue metal analysis of the NAFLD model and control mice groups was performed. Specifically, we quantitatively assessed total levels of copper in the livers of NAFLD mice on HFD and control mice on normal chow using inductively coupled plasma mass spectrometry (ICP-MS) assays (Fig. 5*D*). Copper content in brain, intestine, and kidney tissues was also measured for comparison. In line with the live-animal CCL-1 imaging data as well as literature precedent (24, 60), the ICP-MS experiments verify a deficiency in total hepatic copper in the HFD mice compared with control mice in these endpoint assays. Interestingly, whereas total copper levels in brain and intestine were comparable between the two groups, the HFD mice accumulated higher levels of kidney copper relative to the control mice fed on normal chow. Indeed, copper dysregulation in both diabetic patients and animal models was reported previously to manifest as kidney-centered copper overload with copper deficiency in other tissues, suggesting potential parallels in the contributions of altered copper homeostasis in this diet-induced NAFLD model to diabetes (28, 60).

We next assessed glucose tolerance as a measure of metabolic change in the two groups of animals by monitoring whole-body glucose clearance after i.p. injection of excess glucose (2 mg/g) (Fig. 5*C*). Whereas the mice fed on normal chow were able to process and bring glucose stores back down to basal levels after 2 h, the HFD mice exhibited elevated glucose levels over baseline over the entire course of the test (85 mg/dL above basal levels), confirming a significant impairment in glucose metabolism and validating diet-dependent disease induction that accompanies copper deficiency.

Finally, given the observation of decreased hepatic copper levels in the HFD mice, we sought to identify proteins that could potentially contribute to changes in the status of this metal nutrient within this NAFLD model. Specifically, we characterized expression changes at the protein level for the major copper importer channel Ctr1 and the two major copper export proteins ATP7A and ATPB, as well as the canonical metallochaperone copper chaperone for superoxide dismutase (CCS), owing to the availability of effective antibodies for these targets in Western blot assays. ATP7B serves as the primary transporter for excreting copper from the liver to peripheral tissues, whereas hepatic ATP7A is less studied but has been connected to alterations in copper metabolism (18, 63). As shown by Western blot (Fig. 5*E* and *SI Appendix*, Fig. S15), no major changes in Ctr1 levels were observed in liver tissues between HFD and control diet groups, suggesting that copper deficiency is unlikely to be caused by decreases in copper uptake. In contrast, we observe increases in the expression levels of both ATP7A and ATP7B in the liver extracts of the HFD mice compared with mice fed normal diets, suggesting that the observed copper deficiency in this NAFLD model with high-fat feeding may result from increased export from the liver (Fig. 5*E* and *SI Appendix*, Fig. S15). As expected, CCS levels were elevated in the HFD mice over control diet mice (Fig. 5*E* and *SI Appendix*, Fig. S15). This metallochaperone for Cu/Zn superoxide dismutase is a known marker for alterations in copper metabolism that inversely correlates with intracellular copper bioavailability (64, 65), providing another line of evidence supporting hepatic copper deficiency detected by in vivo CCL-1 imaging and ex vivo ICP-MS.

Concluding Remarks

Like other essential metals, copper can neither be created nor destroyed by the body and, as such, must be carefully regulated to maintain normal physiology. Indeed, loss of copper homeostasis at the organ, tissue, and cellular levels is linked to a broad range of disease pathologies, including anemia, bone loss, hypercholesterolemia, and cardiovascular diseases. However, our understanding of copper mobilization and modulation in various tissues has been limited by the relative dearth of technologies that enable in vivo monitoring of copper dynamics in the same living animal over time, as traditional methods rely largely on endpoint ex vivo assays. To meet this need, we have developed CCL-1, a bioluminescent-based probe that is capable of tracking real-time changes in labile, loosely bound copper pools in living cells and organisms. The high selectivity and sensitivity of CCL-1 for copper coupled with genetic targeting of the firefly luciferase reporter offers a general approach for visualizing changes in localized pools of labile copper in living cells and animals. Applying this unique chemical technology to tissue-specific in vivo copper imaging in mammalian animal models, we identify an imbalance in copper homeostasis in a diet-induced murine model of NAFLD that manifests as a hepatic copper deficiency. Because this method allows for monitoring of labile copper status in the same animals over time, we are able to directly observe a decrease of hepatic copper in vivo at early stages of high-fat feeding before many symptoms of NAFLD manifest, suggesting that changes in copper metabolism may influence metabolic factors involved in disease acquisition and progression. This hepatic copper deficiency is further corroborated by endpoint ex vivo tissue analysis by ICP-MS that shows lower total copper levels in liver tissues of mice fed HFDs versus control mice fed normal chow, as well as characterization of expression changes in major copper homeostasis proteins that are consistent with the notion that copper deficiency correlates with up-regulation of the major copper exporter proteins ATP7A and ATP7B. The time course evaluation of hepatic copper status with CCL-1, as well as the ability to direct the signal output to specific cell and tissue populations with targeted luciferase expression, emphasizes the utility of this approach to illuminate dynamic biology of copper in a targeted location in the same living animal over time. More generally, we envisage that this strategy will lead to a broader range of bioluminescent reporters through modular substitution of analyte-sensitive and biochemically-sensitive triggers onto the luciferin molecule, which would greatly expand the number of available chemical probes for studying molecular signaling and stress agents in animal models of health, aging, and disease.

Materials and Methods

Full materials and procedures for the synthesis of compounds, spectroscopic characterization, cellular imaging, animal experiments, and tissue analysis are described in *SI Appendix*. All animal studies were approved by and performed according to the guidelines of the Animal Care and Use Committee of the University of California, Berkeley.

ACKNOWLEDGMENTS. We thank National Institutes of Health (NIH) (Grant GM79465 to C.J.C. and Grant R01DK101293 to A.S.) for support. M.C.H. thanks the University of California President's Postdoctoral Program for a fellowship, and H.Y.A.-Y. acknowledges the Croucher Foundation for a postdoctoral fellowship. C.M.A. thanks the John and Fannie Hertz Foundation for a graduate fellowship and was partially supported by NIH Chemical Biology Training Grant T32 GM066698. C.J.C. is an Investigator with the Howard Hughes Medical Institute.

1. Ferguson-Miller S, Babcock GT (1996) Heme/copper terminal oxidases. *Chem Rev* 96(7):2889–2908.
2. Ishida S, Andreux P, Poitry-Yamate C, Auwerx J, Hanahan D (2013) Bioavailable copper modulates oxidative phosphorylation and growth of tumors. *Proc Natl Acad Sci USA* 110(48):19507–19512.
3. McCord JM, Fridovich I (1969) Superoxide dismutase. An enzymic function for erythrocuprein (hemocuprein). *J Biol Chem* 244(22):6049–6055.
4. Reddi AR, Culotta VC (2013) SOD1 integrates signals from oxygen and glucose to repress respiration. *Cell* 152(1-2):224–235.
5. Kohen A, Klinman JP (1998) Enzyme catalysis: Beyond classical paradigms. *Acc Chem Res* 31(7):397–404.
6. Herranz N, et al. (2012) Lysyl oxidase-like 2 deaminates lysine 4 in histone H3. *Mol Cell* 46(3):369–376.
7. Brady DC, et al. (2014) Copper is required for oncogenic BRAF signalling and tumorigenesis. *Nature* 509(7501):492–496.
8. Turski ML, et al. (2012) A novel role for copper in Ras/mitogen-activated protein kinase signaling. *Mol Cell Biol* 32(7):1284–1295.
9. Chang CJ (2015) Searching for harmony in transition-metal signaling. *Nat Chem Biol* 11(10):744–747.
10. Dodani SC, et al. (2014) Copper is an endogenous modulator of neural circuit spontaneous activity. *Proc Natl Acad Sci USA* 111(46):16280–16285.
11. Krishnamoorthy L, et al. (2016) Copper regulates cyclic-AMP-dependent lipolysis. *Nat Chem Biol* 12(8):586–592.
12. You H, et al. (2012) Aβ neurotoxicity depends on interactions between copper ions, prion protein, and N-methyl-D-aspartate receptors. *Proc Natl Acad Sci USA* 109(5): 1737–1742.
13. Kaler SG (2011) ATP7A-related copper transport diseases-emerging concepts and future trends. *Nat Rev Neurol* 7(1):15–29.
14. Camakaris J, Voskoboinik I, Mercer JF (1999) Molecular mechanisms of copper homeostasis. *Biochem Biophys Res Commun* 261(2):225–232.
15. Puig S, Thiele DJ (2002) Molecular mechanisms of copper uptake and distribution. *Curr Opin Chem Biol* 6(2):171–180.
16. Aron AT, Ramos-Torres KM, Cotruvo JA, Jr, Chang CJ (2015) Recognition- and reactivity-based fluorescent probes for studying transition metal signaling in living systems. *Acc Chem Res* 48(8):2434–2442.
17. Kozlowski H, Janicka-Klos A, Brasun J (2009) Copper, iron, and zinc ions homeostasis and their role in neurodegenerative disorders (metal uptake, transport, distribution and regulation). *Coord Chem Rev* 253(21-22):2665–2685.
18. Wang Y, Hodgkinson V, Zhu S, Weisman GA, Petris MJ (2011) Advances in the understanding of mammalian copper transporters. *Adv Nutr* 2(2):129–137.
19. Huster D, Lutsenko S (2007) Wilson disease: Not just a copper disorder. Analysis of a Wilson disease model demonstrates the link between copper and lipid metabolism. *Mol Biosyst* 3(12):816–824.
20. Desai V, Kaler SG (2008) Role of copper in human neurological disorders. *Am J Clin Nutr* 88(3):855S–858S.
21. Carr TP, Lei KY (1990) High-density lipoprotein cholesteryl ester and protein catabolism in hypercholesterolemic rats induced by copper deficiency. *Metabolism* 39(5): 518–524.
22. Stättermayer AF, et al. (2015) Hepatic steatosis in Wilson disease—Role of copper and PNPLA3 mutations. *J Hepatol* 63(1):156–163.
23. Huster D, et al. (2007) High copper selectively alters lipid metabolism and cell cycle machinery in the mouse model of Wilson disease. *J Biol Chem* 282(11):8343–8355.
24. Aigner E, et al. (2010) A role for low hepatic copper concentrations in nonalcoholic fatty liver disease. *Am J Gastroenterol* 105(9):1978–1985.
25. Aigner E, et al. (2008) Copper availability contributes to iron perturbations in human nonalcoholic fatty liver disease. *Gastroenterology* 135(2):680–688.
26. Aigner E, Weiss G, Datz C (2015) Dysregulation of iron and copper homeostasis in nonalcoholic fatty liver. *World J Hepatol* 7(2):177–188.
27. Feldman A, Aigner E, Weghuber D, Paulmichl K (2015) The potential role of iron and copper in pediatric obesity and nonalcoholic fatty liver disease. *BioMed Res Int* 2015(2):287401.
28. Gong D, et al. (2008) A copper(II)-selective chelator ameliorates diabetes-evoked renal fibrosis and albuminuria, and suppresses pathogenic TGF-β activation in the kidneys of rats used as a model of diabetes. *Diabetologia* 51(9):1741–1751.
29. Engle TE (2011) Copper and lipid metabolism in beef cattle: A review. *J Anim Sci* 89(2): 591–596.
30. Burkhead JL, Lutsenko S (2013) *The Role of Copper as a Modifier of Lipid Metabolism*. Available at www.intechopen.com/books/lipid-metabolism/the-role-of-copper-as-a-modifier-of-lipid-metabolism. Accessed November 12, 2016.
31. Fahrni CJ (2013) Synthetic fluorescent probes for monovalent copper. *Curr Opin Chem Biol* 17(4):656–662.
32. Cotruvo JA, Jr, Aron AT, Ramos-Torres KM, Chang CJ (2015) Synthetic fluorescent probes for studying copper in biological systems. *Chem Soc Rev* 44(13):4400–4414.
33. Ramos KM, Kolemen S, Chang CJ (2016) Thioether coordination chemistry for molecular imaging of copper in biological systems. *Isr J Chem* 56(9-10):724–737.
34. Bourassa D, et al. (2014) 3D imaging of transition metals in the zebrafish embryo by X-ray fluorescence microtomography. *Metallomics* 6(9):1648–1655.
35. Torres JB, et al. (2016) PET Imaging of copper trafficking in a mouse model of Alzheimer disease. *J Nucl Med* 57(1):109–114.
36. Hong-Hermesdorf A, et al. (2014) Subcellular metal imaging identifies dynamic sites of Cu accumulation in Chlamydomonas. *Nat Chem Biol* 10(12):1034–1042.
37. Peng F (2014) Positron emission tomography for measurement of copper fluxes in live organisms. *Ann N Y Acad Sci* 1314:24–31.
38. Que EL, et al. (2009) Copper-responsive magnetic resonance imaging contrast agents. *J Am Chem Soc* 131(24):8527–8536.
39. Hirayama T, Van de Bittner GC, Gray LW, Lutsenko S, Chang CJ (2012) Near-infrared fluorescent sensor for in vivo copper imaging in a murine Wilson disease model. *Proc Natl Acad Sci USA* 109(7):2228–2233.
40. Li J, Chen L, Du L, Li M (2013) Cage the firefly luciferin!—A strategy for developing bioluminescent probes. *Chem Soc Rev* 42(2):662–676.
41. Paley MA, Prescher JA (2014) Bioluminescence: A versatile technique for imaging cellular and molecular features. *MedChemComm* 5(3):255–267.
42. Prescher JA, Contag CH (2010) Guided by the light: Visualizing biomolecular processes in living animals with bioluminescence. *Curr Opin Chem Biol* 14(1):80–89.
43. Kircher MF, Gambhir SS, Grimm J (2011) Noninvasive cell-tracking methods. *Nat Rev Clin Oncol* 8(11):677–688.
44. O'Neill K, Lyons SK, Gallagher WM, Curran KM, Byrne AT (2010) Bioluminescent imaging: A critical tool in pre-clinical oncology research. *J Pathol* 220(3):317–327.
45. Van de Bittner GC, Bertozzi CR, Chang CJ (2013) Strategy for dual-analyte luciferin imaging: In vivo bioluminescence detection of hydrogen peroxide and caspase activity in a murine model of acute inflammation. *J Am Chem Soc* 135(5):1783–1795.
46. Godinat A, et al. (2013) A biocompatible in vivo ligation reaction and its application for noninvasive bioluminescent imaging of protease activity in living mice. *ACS Chem Biol* 8(5):987–999.
47. Van de Bittner GC, Dubikovskaya EA, Bertozzi CR, Chang CJ (2010) In vivo imaging of hydrogen peroxide production in a murine tumor model with a chemoselective bioluminescent reporter. *Proc Natl Acad Sci USA* 107(50):21316–21321.
48. Sellmyer MA, et al. (2013) Visualizing cellular interactions with a generalized proximity reporter. *Proc Natl Acad Sci USA* 110(21):8567–8572.
49. Porterfield WB, Jones KA, McCutcheon DC, Prescher JA (2015) A "caged" luciferin for imaging cell–cell contacts. *J Am Chem Soc* 137(27):8656–8659.
50. Mofford DM, Adams ST, Jr, Reddy GSKK, Reddy GR, Miller SC (2015) Luciferin amides enable in vivo bioluminescence detection of endogenous fatty acid amide hydrolase activity. *J Am Chem Soc* 137(27):8684–8687.
51. Taki M, Iyoshi S, Ojida A, Hamachi I, Yamamoto Y (2010) Development of highly sensitive fluorescent probes for detection of intracellular copper(I) in living systems. *J Am Chem Soc* 132(17):5938–5939.
52. Au-Yeung HY, Chan J, Chantarojsiri T, Chang CJ (2013) Molecular imaging of labile iron(II) pools in living cells with a turn-on fluorescent probe. *J Am Chem Soc* 135(40): 15165–15173.
53. Au-Yeung HY, New EJ, Chang CJ (2012) A selective reaction-based fluorescent probe for detecting cobalt in living cells. *Chem Commun (Camb)* 48(43):5268–5270.
54. Park H, et al. (October 11, 2016) A system for in vivo imaging of hepatic free fatty acid uptake. *Gastroenterology*, 10.1053/j.gastro.2016.10.002.
55. Leslie M (2015) The liver's weighty problem. *Science* 349(6243):18–20.
56. Uppal V, Mansoor S, Furuya KN (2016) Pediatric non-alcoholic fatty liver disease. *Curr Gastroenterol Rep* 18(5):24.
57. Lee CH, Lam KSL (June 4, 2016) Managing non-alcoholic fatty liver disease in diabetes: challenges and opportunities. *J Diabetes Invest*, 10.1111/jdi.12534.
58. Rinella ME, et al. (2014) Controversies in the diagnosis and management of NAFLD and NASH. *Gastroenterol Hepatol (N Y)* 10(4):219–227.
59. Hardy T, Oakley F, Anstee QM, Day CP (2016) Nonalcoholic fatty liver disease: Pathogenesis and disease spectrum. *Annu Rev Pathol* 11:451–496.
60. Church SJ, et al. (2015) Deficient copper concentrations in dried-defatted hepatic tissue from ob/ob mice: A potential model for study of defective copper regulation in metabolic liver disease. *Biochem Biophys Res Commun* 460(3):549–554.
61. Sato A, et al. (2010) Antiobesity effect of eicosapentaenoic acid in high-fat/high-sucrose diet-induced obesity: Importance of hepatic lipogenesis. *Diabetes* 59(10): 2495–2504.
62. Wang C-Y, Liao JK (2012) A mouse model of diet-induced obesity and insulin resistance. *Methods Mol Biol* 821:421–433.
63. Kim B-E, et al. (2010) Cardiac copper deficiency activates a systemic signaling mechanism that communicates with the copper acquisition and storage organs. *Cell Metab* 11(5):353–363.
64. Bertinato J, Iskandar M, L'Abbé MR (2003) Copper deficiency induces the upregulation of the copper chaperone for Cu/Zn superoxide dismutase in weanling male rats. *J Nutr* 133(1):28–31.
65. Prohaska JR, Broderius M, Brokate B (2003) Metallochaperone for Cu,Zn-superoxide dismutase (CCS) protein but not mRNA is higher in organs from copper-deficient mice and rats. *Arch Biochem Biophys* 417(2):227–234.